

Conjugated Materials

Twisting the TAPPs: Bay-Substituted Non-planar Tetraazaperopyrenes and their Reduced Anions

Benjamin A. R. Günther,^[a] Sebastian Höfener,^[b] Ute Zschieschang,^[c] Hubert Wadepohl,^[a] Hagen Klauk,^[c] and Lutz H. Gade^{*[a]}

Abstract: A new synthesis of tetraazaperopyrenes (TAPPs) starting from a halogenated perylene derivative 3,4,9,10-tetrabromo-1,6,7,12-tetrachloroperylene (1) gave access to bay-substituted TAPPs for the first time. Selective lithiation of the bromine-positions and subsequent addition of tosyl azide led to the formation of the tetraazidotetrachloroperylene (2), which was subsequently reduced by addition of sodium borohydride to the corresponding tetraaminotetrachloroperylene (3). Oxidation to its semiquinoidal form 4 and subsequent cyclization with acid chlorides gave rise to a series of bay-chlorinated TAPPs. Whereas the aromatic core of the previously studied *ortho*-substituted TAPPs was found to be planar, the steric pressure of the two chlorine substituents on each side leads to the twist of the peropyrene core

of approximately 30 degrees, a structural feature also observed in other bay-substituted perylene derivatives. An experimental and computational analysis reveals that introducing chloride substituents at these positions leads to slightly increased electron affinities (EA) enabling the selective generation and characterization of the reduced mono-anionic radicals and closed shell di-anionic species. These anions were isolated and characterized by UV/Vis spectroscopy and EPR or NMR, respectively. Processing of the bay-chlorinated TAPPs in n-channel organic TFTs revealed electron mobilities of 0.001 to 0.003 cm²V⁻¹s⁻¹. These reduced electron mobilities compared to the *ortho*-halogenated TAPPs are thought to be rooted in the less densely packed solid-state structures.

Introduction

Perylene tetracarboxydiimides (PDIs) have been extensively studied as functional dyes and electronic materials.^[1–17] Their properties may be varied widely by substitution at the perylene core and at the imido-N position. The carboxy substituents at the central perylene core render these materials electron acceptors, and this property in particular has been underlying their application in organic electronics.

Different synthetic approaches have been established to functionalize the *bay*-^[2,10,18–23] or *ortho*-^[24–31] positions selective-

ly or even to fully substitute^[26,32,33] the perylene core in a single-step-reaction (Figure 1).^[34,35]

A class of molecular dyes which has displayed photophysical and redox properties similar to the ubiquitous PDIs are the tetraazaperopyrenes (TAPPs) which have been investigated for more than a decade.^[36–48] Whereas the electron accepting character of the PDIs is due to carboximide substituents at both ends of the perylene core, TAPPs contain two pyrimidine rings fused with the central perylene unit. The electron accepting character of the resulting N-heteropolycycles is thus effectively built into the aromatic core itself rather than substituent-induced. Viewed alternatively, the fourfold isosteric [CH→N] substitution in the parent hydrocarbon peropyrene radically changes its electronic properties while leaving its molecular shape practically unchanged.

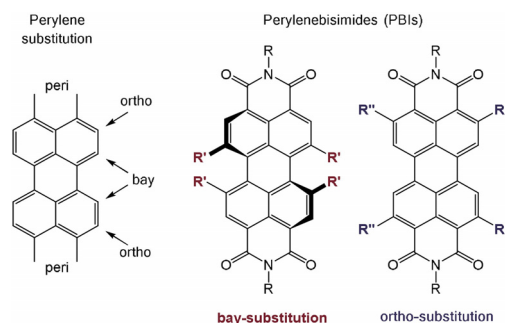


Figure 1. Left: Substituent positions in perylene derivatives. Right: bay- and ortho substitution in PDIs.

[a] B. A. R. Günther, Prof. Dr. H. Wadepohl, Prof. Dr. L. H. Gade
Anorganisch-Chemisches-Institut, Universität Heidelberg
Im Neuenheimer Feld 270, 69120 Heidelberg (Germany)
E-mail: lutz.gade@uni-heidelberg.de

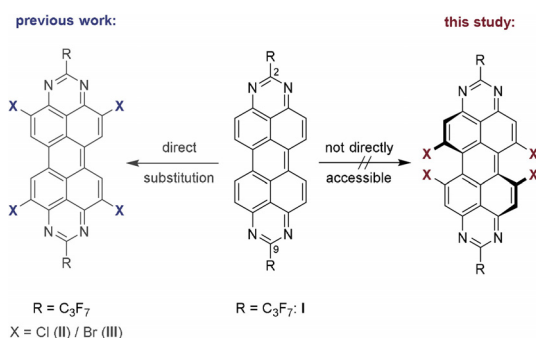
[b] Dr. S. Höfener
Institute of Physical Chemistry
Karlsruhe Institute of Technology (KIT) P.O. Box 6980
76049 Karlsruhe (Germany)

[c] Dr. U. Zschieschang, Dr. H. Klauk
Max Planck Institute for Solid State Research
Heisenbergstr. 1, 70569 Stuttgart (Germany)

Supporting information and the ORCID identification number(s) for the author(s) of this article can be found under:
<https://doi.org/10.1002/chem.201903413>.

© 2019 The Authors. Published by Wiley-VCH Verlag GmbH & Co. KGaA. This is an open access article under the terms of the Creative Commons Attribution License, which permits use, distribution and reproduction in any medium, provided the original work is properly cited.

Whereas electrophilic substitution of PDIs and related compounds occurs in the *bay*-positions, the corresponding derivatization of the parent TAPP compounds (**1**) happened exclusively in the *ortho*-position, leaving the *bay*-CH units unaffected and thus maintaining the planar structure of the aromatic core (Scheme 1).^[42,44] Manifold derivatization of TAPP derivatives in the 2,9-positions, as well as in the *ortho*-position, has led to a detailed understanding of the molecular behavior and its photophysical and electronic properties. On the other hand, it has not yet been possible to functionalize the inner *bay* position of the peropyrene core, in order to establish a link with the well established PDI chemistry and its further development towards more complex polycyclic aromatics. Thus, a fundamental part of TAPP-chemistry has remained unexplored to date.



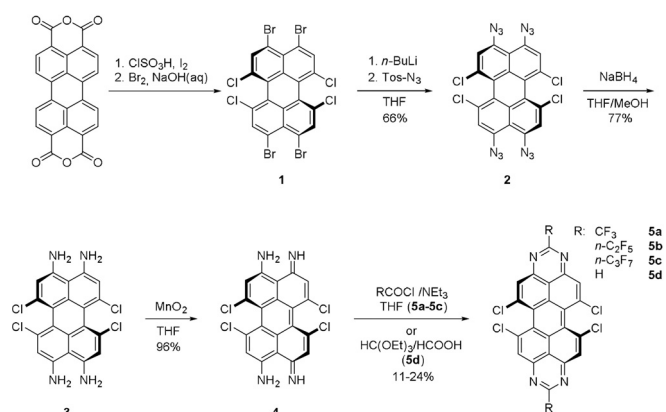
Scheme 1. Approach to synthesize *ortho*-substituted TAPP-derivatives (left, previous work) and inability to functionalize the *bay*-position (right) when starting from earlier parent compound **I**.

In this work, we report a novel TAPP synthesis, which for the first time allowed their *bay* functionalization. Additionally, a detailed study of their reduced species was conducted to gain insights into electronic behavior and their stability. Comparison of the *ortho*- and *bay*-chlorinated TAPPs provided insight into the influence of the different substitution patterns of the peropyrene core.

Results and Discussion

Synthesis of *bay*-chlorinated TAPPs

The starting material for the synthesis of *bay*-substituted TAPPs was tetrabromotetrachloroperylene (**1**), first published in 2014 (Scheme 2).^[49] Selective lithiation of the bromine positions and subsequent addition of tosyl azide led to the formation of the tetraazidotetrachloroperylene (**2**), which was subsequently reduced by addition of sodium borohydride to the corresponding tetraaminotetrachloroperylene (**TAP-Cl**, **3**). Analogous to the previously reported non-chlorinated tetraaminoperylene, this compound displayed a tendency to be oxidized under ambient conditions to form the chlorinated diaminoperylenequinoxaline (**DPDI-Cl**, **4**), however, the reaction proceeded much more slowly than for the parent **DPDI** and occasionally did not go to completion. Therefore, oxidation to the semiqui-



Scheme 2. Synthetic route to the *bay*-chlorinated DPDI analogue (**DPDI-Cl**, **4**) and subsequent ring-closing reaction to the corresponding *bay*-TAPP-Cl **5**.

noidal compound **4** was selectively carried out by the reaction of **3** with activated MnO_2 .

By employing the standard ring-closing reaction conditions of the original TAPP-synthesis, the first *bay*-substituted TAPP derivatives with H- or perfluoroalkyl-substituted 2- and 9-position (**5**) were obtained. As opposed to the planar *ortho*-substituted TAPP derivatives, which only possess low solubility in common organic solvents, the twist induced by the *bay*-chlorination leads to a significantly enhanced solubility.

Crystal structures of **5a-c**

Single crystals of the tetrachlorinated TAPPs **5a**, **5b** and **5c** were grown by slow evaporation of concentrated solutions in chloroform (**5a** and **5c**) and toluene (**5b**) (Figure 2). All three solid-state structures reveal a significant twist between the two diazaphenalenyl subunits of the tetraazaperopyrene core: **5a** (29.4 degrees), **5b** (30.6 degrees) and **5c** (32.4 degrees). Whereas the aromatic core of the previously studied *ortho*-substituted TAPPs was found to be planar, the steric pressure of the two chlorine substituents on each side leads to the twist of the peropyrene core, a structural feature also observed in other *bay*-substituted perylene derivatives.^[18]

In all three cases, the packing pattern in the solid state is determined by intermolecular stacking of two diazaphenalenyl subunits. This motif leads to distances as close as 3.4 Å between the aromatic core halves of two adjacent molecules, however, the general packing pattern varies for the different perfluorinated alkyl chains (Figure 3). Thus, the CF_3 -substituted TAPP **5a** packs in a zigzag fashion, while the elongation of the fluoroalkyl chains in **5b** leads to more columnar-like packing pattern. The crystals of **5c** could not be obtained without co-crystallization of solvent, which renders an assessment of the packing pattern less significant. The key data of the solid-state structures are summarized in Table 1.

Interconversion barrier of atropo-enantiomers

As the steric repulsion between opposing chlorine atoms leads to the aforementioned torsion in the peropyrene backbone, the dye molecules possess helical chirality, leading to *P*- and

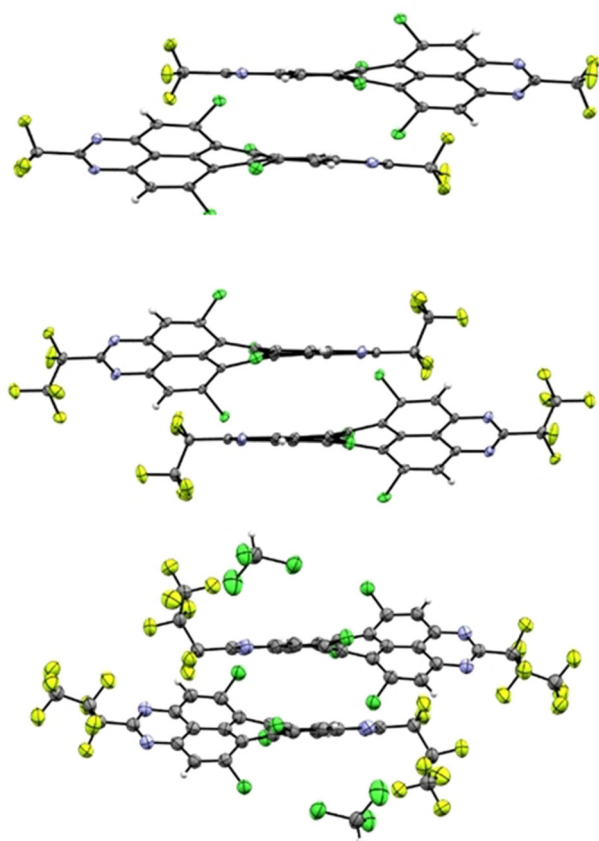


Figure 2. Solid state structure of **5 a** (top), **5 b** (middle) and **5 c** (bottom).

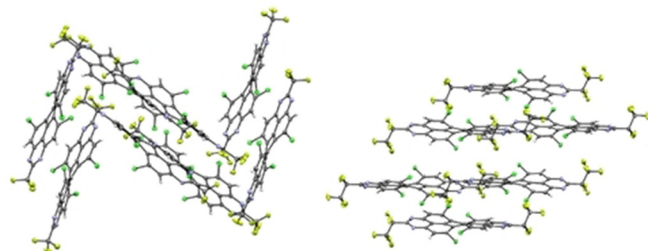
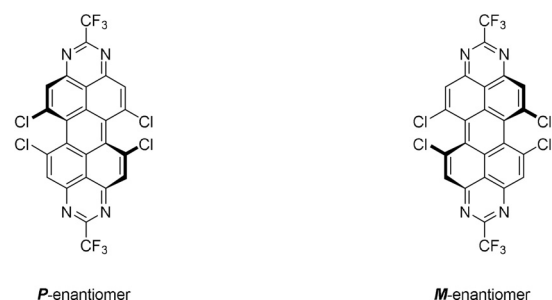


Figure 3. Packing pattern of **5 a** in a zigzag-like fashion (left) and of **5 b** in a columnar pattern (right).

Table 1. Structural parameters of solid-state structures of 5 a–c .				
	Crystal system	Space group	π - π Plane distance [Å] ^[a]	Torsion angle [°] ^[b]
5 a	orthorhombic	<i>Pbca</i>	3.440	29.43 (0.03)
5 b	monoclinic	<i>I2/a</i>	3.535	30.10 (0.03)
5 c	triclinic	<i>P1</i>	3.603 ^[c]	32.44 (0.07)

[a] π - π Distance was measured between two adjacent diazaphenalenyl-subunits. [b] Torsion angle was measured between both diazaphenalenyl-subunits of one molecule. [c] **5 c** co-crystallized with chloroform, but displaying close packing between pairs of molecules.

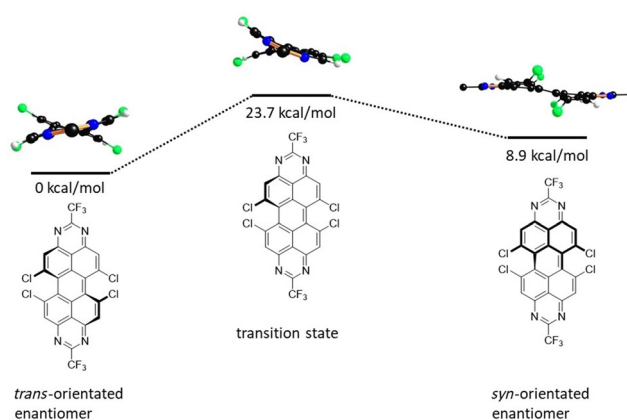
M-atropisomers (Scheme 3). This helical isomerism has been studied in detail for the structurally similar bay-functionalized perylene bisimides,^[23,50–58] and the interconversion barrier between the atropo-enantiomers was found to depend on the



Scheme 3. The two possible *P*- and *M*-enantiomers of bay-substituted TAPPs.

number and steric demand of the bay substituents. Whereas for most PDIs interconversion occurs rapidly at room temperature, larger substituents raise the energy barrier over 22.2 kcal mol⁻¹, which is the minimum barrier required for the isolation of the enantiomers at ambient temperature and the usual timescale of product handling. It was therefore of interest to compare analogously substituted PDI- and TAPP-systems in order to obtain insight into the flexibility of the peropyrene core compared to the PDI system.^[54,59]

To this end, the interconversion of the atropisomeric bay-chlorinated tetraazaperopyrenes, has been modeled theoretically by DFT (Scheme 4). For a potential one-step mechanism involving a planar transition state the energy barrier would be approximately 72 kcal mol⁻¹, thus locking the molecules in a single helical form. As an alternative pathway, the stepwise isomerization was investigated, in which the first transition state is reached via the planarization on only one side of the TAPP, while the opposite side remains in the twisted form. This results in a reduced torsion angle of about 10 degrees compared to 32 degrees in the ground state (Table 2). The computed activation energy was found to be 23.7 kcal mol⁻¹, and the resulting intermediate bay-substituted TAPP is characterized by mutually *syn*-oriented chloro substituents. This achiral intermediate is only 9 kcal mol⁻¹ higher in energy than the *trans*-oriented conformer and either reacts back to the initial form or to the other atropisomer.



Scheme 4. Calculated relative energies of conversion between atropo-isomers in kcal mol⁻¹.

Table 2. Computed relative energies including the zero-point vibrational energy (ZPVE) and angles of intermediates and the transition state (TS) structure.

	E_{ZPVE} [kcal mol ⁻¹]	Torsion angle [°] ^[a]	Imaginary frequency [cm ⁻¹]
<i>trans</i> -oriented enantiomer	0	32	
TS	24	10/31	74.96
<i>syn</i> -oriented intermediate	9	23	

[a] Torsion angle was measured using the four C-atoms in the *bay*-area.

This reaction sequence corresponds to the mechanism, Würthner et al. have proposed for the corresponding PDI-systems.^[54] Notably, the isomerization barrier of the *bay*-chlorinated TAPPs is very similar to that reported for the PDI-Cl₄, which suggests that indeed the PDI-core possesses similar rigidity/flexibility as the polycyclic aromatic core of the TAPP molecules.

UV/Vis absorption and emission spectra

The UV/Vis absorption and emission spectra of the TAPP derivatives **5a–d** recorded in THF are displayed in Figure 4. Similar to the non-twisted *ortho*-substituted TAPP derivatives, the absorption and emission maxima remain unchanged upon variation of the alkyl-substituents in the 2- and 9-positions.^[42]

All derivatives were found to exhibit absorption maxima in the range of 468 to 474 nm with vibrational progressions and emission maxima in the range of 496 to 505 nm. As TAPPs are

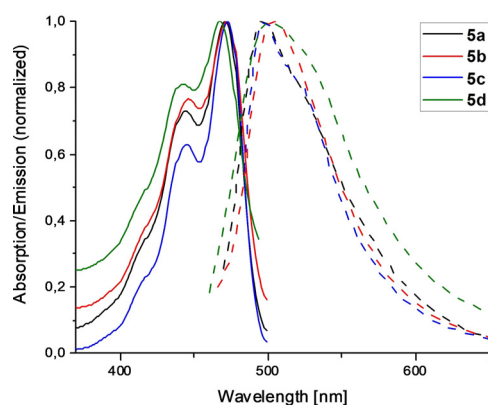


Figure 4. Absorption (continuous line) and emission (dashed line) spectra of *bay*-substituted compounds **5a–d** recorded in THF.

known to aggregate in solution, measurements were repeated in different solvents (DCM and CHCl₃) and in different concentrations. However, identical absorption and emission data were observed, leading to the conclusion, that these twisted TAPPs do not tend to aggregate in common organic solvents. An overview of the optical properties is given in Table 3.

Complementing the measurement of the absorption and emission spectra in solution, Table 3 contains vertical transition energies computed at time-dependent density functional theory (TDDFT) level of theory. While the absolute values of the vertical excitation (VE) and the vertical de-excitation (VD) energies deviate from the measured absorption and emission bands by 0.05 and 0.15 eV, respectively, the table confirms that the photophysical data remain unaffected by the variation of substituents in the 2- and 9-positions.

Since computed vertical electronic transition energies cannot be directly related to the experimental results, we also simulated vibrationally resolved adiabatic transitions.^[48] Simulated absorption and emission spectra of **5d** are displayed in Figure 5. At zero temperature, the simulated spectra show distinct transitions for individual vibronic transitions.

The spectra do not seem to be dominated by the 0–0 transition and they thus display a Stokes shift of 0.02 eV (140 cm⁻¹) at zero temperature, however, the incorporation of temperature effects leads to a Stokes shift of about 0.07 eV (about 586 cm⁻¹) at 300 K. The finite-temperature spectrum furthermore reproduces the general shape of the experimental spectra as shown in Figure 4, which is characterized by a pronounced vibrational progression at lower wavelength for the absorption but only a broadened band for emission. We note that the experimentally observed Stokes shifts are larger compared to the simulated values, which might be due to solvation effects which are not included in the simulations in vacuum.

Redox properties

To assess the redox chemical properties of the *bay*-chlorinated TAPP derivatives cyclic voltammograms (CVs) of all compounds were recorded. They were found to exhibit two individual and fully reversible one-electron reduction steps to the mono-anionic radical species and the subsequent di-anionic compound. In Figure 6, the CV is shown for compound **5b**.

The energies of the lowest unoccupied molecular orbital (LUMO) were estimated by subtraction of the reversible first reduction potentials obtained from the cyclic voltammograms of

Table 3. Photophysical properties of **5a–d** measured in THF and computed vertical electronic excitation (VE) and de-excitation (VD) energies.

	R	λ_{abs} [nm] (log ϵ) ^[a]	λ_{em} [nm] (φ_{Em}) ^[a]	0–0 Transition [nm] ^[b]	Stokes shift [cm ⁻¹]	λ_{VE} [nm] (DFT) ^[c]	λ_{VD} [nm] (DFT) ^[c]
5a	CF ₃	471 (4.57)	496 (0.12)	482	1070	481	534
5b	C ₂ F ₅	472 (4.64)	505 (0.09)	485	1384	482	535
5c	C ₃ F ₇	474 (4.59)	496 (0.10)	484	936	482	536
5d	H	468 (3.98)	501 (0.05)	480	1407	478	532

[a] Absorption and emission spectra were recorded in THF. [b] 0–0-Transition was obtained at the intersection of absorption and emission spectra. [c] Vertical electronic excitation (VE) and de-excitation (VD) energies were calculated using B3LYP as functional and TZVPP as the basis set.

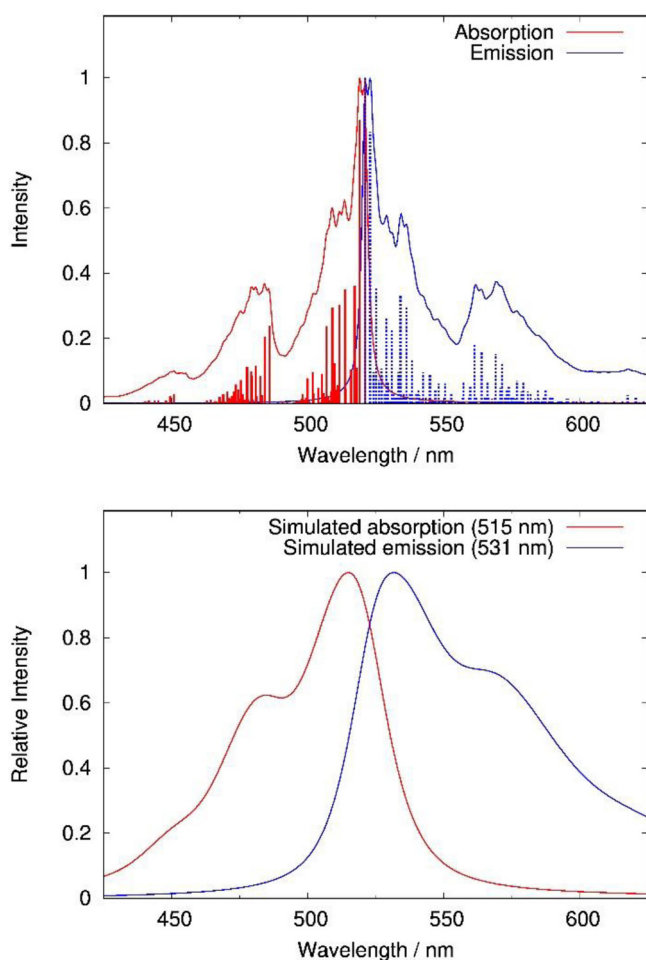


Figure 5. Simulated spectra of compound **5d** at 0 K (top) and 300 K (bottom), shifted according to the theoretical 0-0 transition energy of 521 nm (2.38 eV), computed in the harmonic approximation at B3LYP/def2-TZVPP level of theory employing D_2 symmetry.

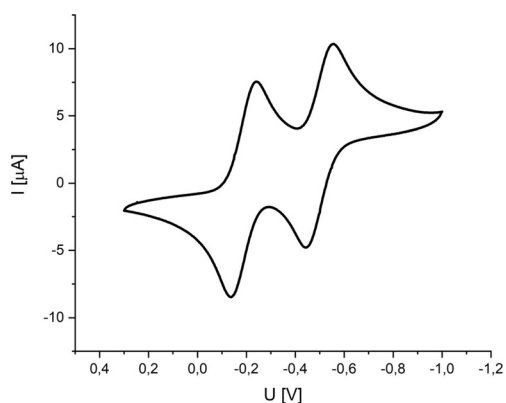


Figure 6. Cyclic Voltammogram of **5b**, measured in DCM, supp. electrolyte Bu_4NPF_6 , reference SCE, sweep rate 50 mV s^{-1} .

the redox potential of ferrocene (4.8 eV for Fc/Fc^+).^[60] As expected, the substituents in the 2- and 9-position have only limited influence on the frontier orbitals, similar to the UV/Vis absorption and emission spectra discussed above. This was

backed up by the computational determination of the Kohn–Sham frontier orbital energies determined by DFT.

Whereas the energies of the LUMO and the highest occupied molecular orbital (HOMO) of derivatives **5a–c** are almost identical at around -4.15 eV , the “removal” of the perfluorinated alkyl group leads to an increase of both the HOMO and LUMO energies by about 0.5 eV, resulting in a virtual identical HOMO–LUMO gap of all derivatives. Visualization of the frontier orbitals (Figure 7), reveals the nodal planes of the frontier orbitals along the principal molecular axis in which the substituents in the 2- and 9-positions are located. This also explains the nearly identical absorption and emission spectra of **5a–d** which are dominated by the HOMO–LUMO transition.

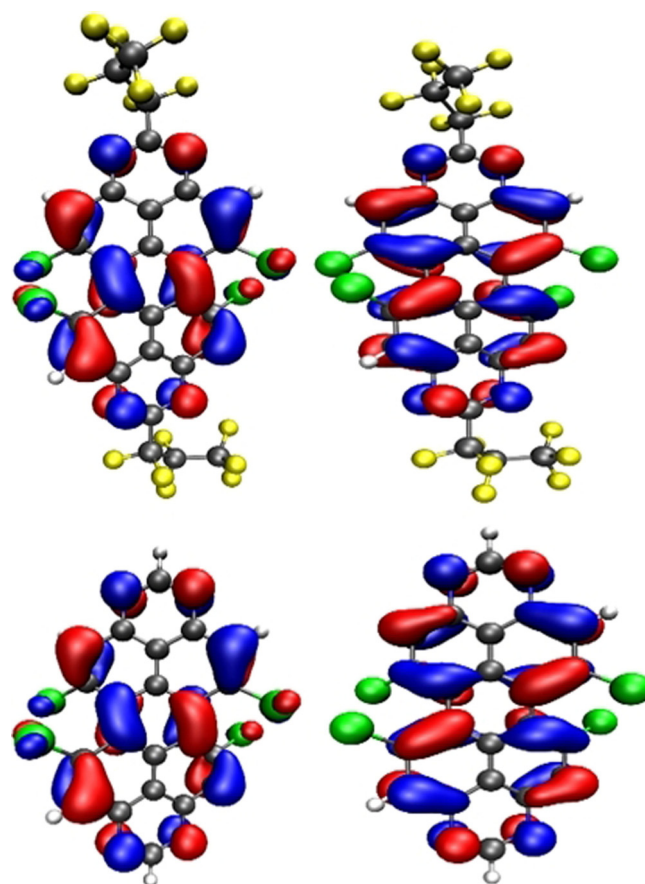


Figure 7. Visualization of the HOMO (left) and LUMO (right) of **5c** (top) and **5d** (bottom); level of theory used is B3LYP/def2-SVP, isovalue 0.03.

For the perfluorinated alkyl groups electron affinities between 3.21 and 3.31 eV were found for **5a–c**, whereas the hydrogen-substituted compound **5d** was found to possess a significantly reduced electron affinity of about 2.73 eV (Table 4). These adiabatic EA values do not differ significantly from vertical EA values obtained from GW methods (The GW method is a way to correct artefacts in Kohn–Sham (KS) methods which employ exchange–correlation (XC) functionals),^[61] see Table 2, which indicates that the one-electron reduction does not induce a significant change in the molecular geometry. This corresponds to a small reorganization energy which is desira-

Table 4. Adiabatic electron affinities (aEA) obtained from the Δ SCF approach, vertical electron affinities (vEA) from the GW method, and frontier orbital energies of compounds **5a–d**.

R	aEA _(ΔSCF) [eV] ^[a]	vEA _(GW) [eV] ^[a]	E_{HOMO} (DFT) [eV] ^[a]	$E_{\text{HOMO-LUMO}}$ [eV]	E_{LUMO} (DFT) [eV] ^[a]	E_{LUMO} (exp, CV) [eV] ^[b]
5a CF ₃	3.23	3.21	−6.84	2.71	−4.12	−4.14
5b C ₂ F ₅	3.22	3.25	−6.86	2.71	−4.15	−4.21
5c C ₃ F ₇	3.31	3.27	−6.91	2.71	−4.20	−4.20
5d H	2.73	2.75	−6.43	2.72	−3.71	−3.93

[a] Properties were calculated using B3LYP as the functional and a def2-QZVPP as basis set. [b] LUMO energy was estimated from the reversible first reduction potentials obtained from the cyclic voltammograms using the redox potential of ferrocene as reference (4.8 eV for Fc/Fc⁺).^[60]

ble for electron transporting compounds with large λ_+ (reorganization energy for hole transport) and small λ_- (reorganization energy for electron transport).^[62]

The two individual one-electron reduction steps occurring consecutively were monitored for **5a** by UV/Vis spectroscopy in a spectroelectrochemical cell (Figure 8). By applying a po-

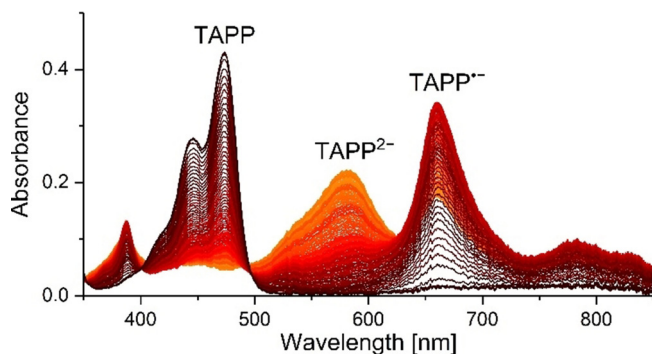
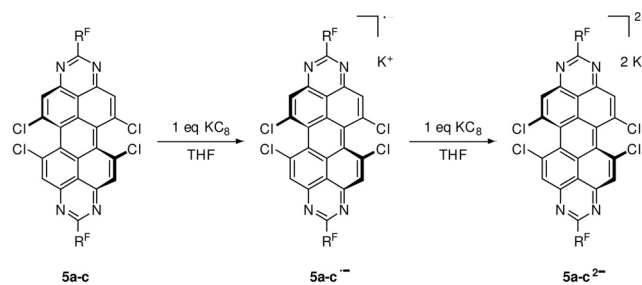


Figure 8. Absorption spectra of the two individual reduction steps of **5a** in THF; voltage steps from 0 V (black) via −0.5 V (red) to −1.0 V (orange).

tential of −0.5 V the absorption band at 474 nm of the neutral compound completely disappeared, while the formation of a green species with a long-wavelength absorption maximum at 663 nm was detected. This can be attributed to the monoanionic radical TAPP^{•−}. The further lowering of the reduction potential to −1.0 V led to the second reduction step, observable by a change of color to purple and the hypsochromic shift of the absorption band to 663 nm. The spectra exhibit relatively well defined isobestic points at 400 nm and 495 nm, indicating that both reduction steps proceed cleanly and without significant further conversions.

The two reduced TAPP species, TAPP^{•−} and TAPP^{2•−}, of **5a–5c** could also be isolated quantitatively by addition of one or two equivalents of KC₈, respectively (Scheme 5). The radical monoanionic TAPP-compounds were characterized by EPR (Figure 9), which for all derivatives possess a *g*-factor of 2.004, which is to be expected for radical organic compounds. Unfortunately, hyperfine couplings were only partially resolved precluding a complete simulation of the spectra.



Scheme 5. Reduction of **5a–c** to the radical monoanionic (**5a–c^{•−}**) or diamagnetic dianionic TAPP (**5a–c^{2•−}**) using KC₈.

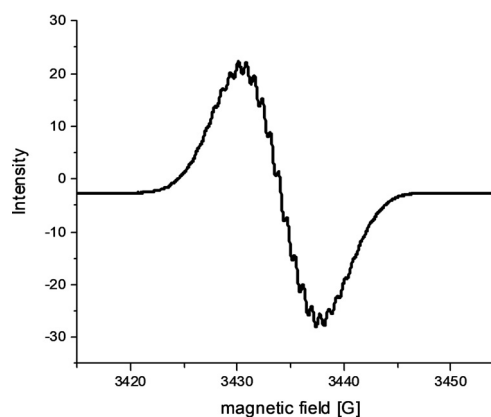


Figure 9. EPR-spectrum (THF, r.t.) of **5b**.

None of the radical monoanions showed any signs of degradation under inert atmosphere, and even under ambient conditions the radicals only degraded very slowly, over a period of weeks, in the solid state. The insertion of the second electron led to a diamagnetic species, which allowed the compounds to be characterized by standard NMR methods, performed exemplarily for compound **5a**. Both ¹H NMR spectra and ¹⁹F NMR spectra display a shift of their signals to a higher field probably due to the enhanced electronic shielding by the additional electrons (Supporting Information). Also, the UV/Vis absorption spectra were recorded for each species, which reproduced the results of the spectroelectrochemical investigation depicted in Figure 8 (Supporting Information).

Bay-chlorinated TAPPs as n-channel semiconductors

Ortho-substituted TAPP derivatives have been successfully employed as semiconductors in n-channel organic TFTs, exhibiting electron mobilities of up to 0.17 cm²V^{−1}s^{−1}.^[63] In analogy, the bay-substituted TAPPs **5a–c** were evaluated in bottom-gate, top-contact TFTs with a vacuum-deposited semiconductor layer (Table 5). The TFTs consisted of a doped silicon substrate that also served as a common gate electrode, a stack of thermally grown SiO₂, atomic-layer-deposited Al₂O₃ and a self-assembled monolayer (SAM) of *n*-tetradecylphosphonic acid as the gate dielectric, and shadow-mask-patterned Au top contacts (a detailed description of the fabrication process can be

Table 5. Summary of the transistor parameters electron field-effect mobility (μ_n), on/off current ratio (I_{on}/I_{off}), threshold voltage (V_{th}), subthreshold swing (SS) and temperature (T) measured under ambient conditions.

	I_{on}/I_{off}	V_{th} [V]	SS [V dec $^{-1}$]	T [°C]	μ_n [cm 2 Vs $^{-1}$]
5a	10 4	6	1.9	70	0.002
5b	10 4	19	2.8	40	0.003
5c	10 4	13	4.4	90	0.001

found in the Supporting Information). In all cases, n-channel semiconducting behavior was observed, with electron mobilities of 0.001 to 0.003 cm 2 V $^{-1}$ s $^{-1}$.

The atomic force microscopy (AFM) images of the vacuum-deposited TAPP films reveal a low tendency of self-organization. The films of **5a** and **5c** are essentially amorphous, and only **5b** shows a locally crystalline structure in certain areas of the image (Figure 10), which may explain the relatively low electron mobilities.

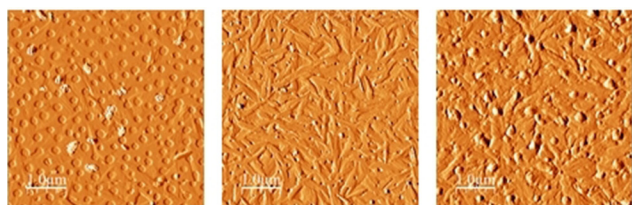


Figure 10. Atomic force microscopy (AFM) images of vacuum-deposited films of **5a** (left), **5b** (middle) and **5c** (right).

In all cases, variation of the substrate temperature during the semiconductor deposition did not lead to an improvement of the self-organization of the material. On the other hand, the reduced tendency to pack in tight units, however, may open opportunities for the TAPP chemistry to explore new fields of applications. Also, the increased solubility associated with the reduced packing density is expected to be beneficial for solution processing.

Ortho- versus bay-substitution

To further understand the different influence of *ortho*- and *bay*-substitution in TAPP derivatives, the two core-chlorinated TAPP isomers **5c** and **II** shall be compared. The absorption maxima at 474 nm (**5c**) and 469 nm (**II**) of both isomers indicate that the bathochromic shift, induced by the chlorine substitution, is almost equally pronounced (Figure 11). However, the emission maximum of the *bay*-substituted derivative is red-shifted by 15 nm compared to the *ortho*-substituted TAPP, resulting in a Stokes shift for **5c** of 936 cm $^{-1}$ which is almost twice as large as observed for **II** (445 cm $^{-1}$). Additionally, the high fluorescence quantum yield of the *ortho*-chlorinated **II** (0.78) is reduced to 0.10 for the twisted *bay*-chlorinated TAPP **5c** which appears to be characterized by more accessible internal degrees of freedom and thus enhanced non-radiative relaxation processes.

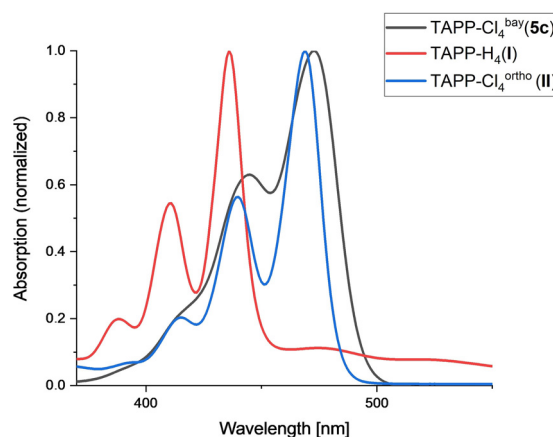


Figure 11. Absorption spectra of unsubstituted TAPP I (red), *ortho*-chlorinated TAPP II (blue) and *bay*-chlorinated TAPP **5c** (black) in THF.

The comparison of the electrochemical properties also reveals some significant differences between **5c** and **II** (Figure 12). The LUMO-level of both chlorinated isomers at -4.20 eV (**5c**) and -4.03 eV (**II**) is significantly stabilized compared to the unsubstituted compound **I** (-3.66 eV), however,

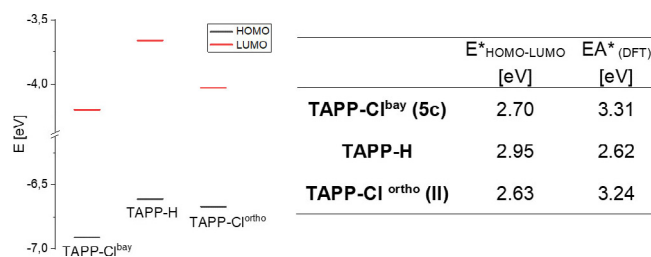


Figure 12. Calculated HOMO- and LUMO-levels (left) and HOMO-LUMO-gaps and EA (right) of **I**, **II** and **5c**.

this effect is even more pronounced for the *bay*-substituted TAPP **5c**. In contrast to the *ortho*-chlorinated derivative **II**, the *bay*-substitution additionally leads to a stabilization of the HOMO level, leading again to similar HOMO-LUMO gaps of 2.70 eV (**5c**) and 2.63 eV (**II**). The electron affinity, which is also a key parameter in the evaluation of potential n-channel semiconductors, is higher for the *bay* substitution (3.31 eV) compared to the *ortho* substitution (3.09 eV). Overall, *bay*-chlorination leads to a greater stability of the anionic (radical) species compared to the *ortho*-substituted constitutional isomers.

Whereas both, the photophysical and the electronic properties are similar for both TAPP-Cl isomers, the change of molecular geometry resulting from the different substitution patterns, is significant. Whereas the planar peropyrene core is barely affected by the *ortho*-substitution, the steric repulsion of the *bay* substituents leads to a large twist of approximately 30 degrees between the two subunits of the TAPP. This difference in molecular structure gives rise to an organized and dense packing pattern in case of the *ortho*-substituted derivative **II** in its solid-state structure (with intermolecular distances

of 3.38 Å), whereas this type of packing is disrupted for the *bay*-substituted derivative **5c** leading to reduced electron mobilities while the molecular redox properties are virtually unchanged. Conversely, the reduced long-range order, leads to a significantly increased solubility and potential processability of the *bay*-substituted molecules.

Conclusions

In this study we have expanded the chemistry of tetraazaperopyrenes (TAPPs) to include non-planar *bay*-chlorinated derivatives. This required a new synthetic strategy which was based on previous work in perylene chemistry and required the introduction of the condensed pyrimidine units to the central perylene core in the final reaction steps. As expected from previous studies of perylene bisimides, the *bay*-chlorinated TAPPs possess a twisted aromatic core due the steric pressure of the *bay*-substituents. In contrast to the previously studies *ortho*-substituted TAPPs, these new compounds allowed facile reduction to the monoanionic radical, which was found to be remarkably stable at ambient conditions. Further reduction gave thermally stable dianionic species which were characterized in solution. Both anionic species were characterized by UV/Vis, EPR and NMR spectroscopy, and theoretical modelling. The present work allows for the first time not only to fine-tune the electronic properties of TAPPs, but simultaneously adjust the geometric properties in a complementary fashion.

Experimental Section

The syntheses were performed under dried argon in standard Schlenk glassware, which was flame-dried prior to use. Solvents were dried according to standard procedures. The ¹H-, ¹³C- and ¹⁹F-NMR spectra were recorded with Bruker AVANCE 400 and 600II+ spectrometers equipped with variable-temperature units. ¹H signals (CDCl₃: 7.26 ppm, [D₈]THF: 1.72 ppm/3.58 ppm, [D₆]DMSO: 2.50 ppm) and ¹³C-signals (CDCl₃: 77.16 ppm, [D₈]THF: 67.21 ppm/25.31 ppm, [D₆]DMSO: 39.52 ppm) were referenced according to standard literature values.^[64] The MALDI mass spectra were obtained from a Bruker apex-Qe FT-ICR spectrometer and a Bruker Autoflex Speed MALDI-TOF spectrometer. The absorption spectra were recorded on a Cary 500 UV/Vis/NIR spectrophotometer and were baseline and solvent corrected. Emission spectra were measured on a Varian Cary Eclipse Spectrophotometer. Description how Fluorescence quantum yields were obtained is explained in detail in the Supporting Information. Cyclic voltammetry was conducted using a standard commercial electrochemical analyser in a three-electrode single-component cell under inert atmosphere. The working electrode consists of a platinum disk, the counter electrode of a platinum wire and a saturated calomel electrode was used as a reference electrode. As internal reference ferrocene was used in all cases. As supporting electrolyte 0.1 M tetrabutylammonium hexafluorophosphate was used.

3,4,9,10-Tetrabromo-1,6,7,12-tetrachloroperylene (**1**) was synthesized according to the literature procedures.¹ All other starting materials were obtained commercially and used without further purification.

Preparation of compound 2

3,4,9,10-Tetrabromo-1,6,7,12-tetrachloroperylene (2.00 g, 2.83 mmol, 1 equiv.) was suspended in THF (200 mL) and *n*-butyllithium (7.94 mL, 2.5 M in hexane, 19.8 mmol, 7 equiv.) were added dropwise at -78 °C. After stirring at this temperature for one hour a solution of Tosyl azide (5.59 g, 28.4 mmol, 10 equiv.) in THF (5 mL) was added dropwise and the reaction mixture was allowed to warm up to r.t. overnight. After the addition of H₂O (30 mL), the phases were separated and the aqueous phase was extracted with DCM (3 × 100 mL). The united organic phases were dried over Na₂SO₄ and evaporation of the solvent gave the crude product, which was further washed with MeOH, acetonitrile and pentane to yield **2** as a red solid (0.75 g, 1.35 mmol, 66%). ¹H NMR (600.13 MHz, CDCl₃, 295 K): δ [ppm] = 7.35 (s, 4H). ¹³C NMR (150.90 MHz, CDCl₃, 295 K): δ [ppm] = 114.6, 119.4, 122.1, 133.6, 136.6, 136.7.

Preparation of compound 3

Sodium borohydride (0.221 g, 5.85 mmol, 2.7 equiv.) was added to a solution of **2** (1.20 g, 2.17 mmol, 1 equiv.) in THF (72 mL) and MeOH (6 mL). The reaction mixture was stirred at r.t. for two hours. The reaction was quenched by the addition of 2 M HCl (1.20 mL), stirred for 30 minutes and subsequently aqueous 2 M NaOH (1.20 mL) was added. The solvent was removed in vacuo and the remaining solid was washed with water, MeOH, acetonitrile and pentane and dried in vacuo to give **3** as a red solid (0.75 g, 1.67 mmol, 77%). ¹H NMR (600.13 MHz, [D₈]THF, 295 K): δ [ppm] = 5.43 (s, 8H), 6.65 (s, 4H). ¹³C-NMR (150.90 MHz, [D₆]DMSO, 295 K): δ [ppm] = 113.4, 123.5, 125.8, 136.4, 146.5, 159.5. HRMS (MALDI⁻): calcd for C₂₀H₁₂³⁵Cl₃³⁷Cl₁N₄ [M]⁺: 449.9787, found: 449.9781.

Preparation of compound 4

MnO₂ (3.00 g, 34.5 mmol, 20.7 equiv.) was added to a solution of **3** (0.75 g, 1.67 mmol, 1 equiv.) in THF (250 mL). After stirring for one hour at r.t., the reaction mixture was filtered over Celite and the solvent was removed in vacuo to give the product **3** as a green solid (0.72 mg, 1.67 mmol, 96%). ¹H NMR (600.13 MHz, [D₆]DMSO, 295 K): δ [ppm] = 7.30 (s, 4H), 9.19 (bs, 4H), 10.48 (bs, 2H). ¹³C NMR (150.90 MHz, [D₆]DMSO, 295 K): δ [ppm] = 101.2, 122.8, 125.0, 134.6, 158.2. HRMS (MALDI⁻): calcd for C₂₀H₁₀³⁵Cl₃³⁷Cl₁N₄ [M]⁺: 447.9630; found: 447.9656.

Preparation of compound 5a

Triethylamine (435 μL, 3.12 mmol, 2.8 equiv.) and trifluoroacetic anhydride (374 μL, 2.79 mmol, 2.5 equiv.) were added to a solution of DPDI-Cl (**4**) (500 mg, 1.12 mmol, 1 equiv.) in THF (10 mL) and the reaction mixture was refluxed for 72 h. After cooling to r.t., the volatiles were removed in vacuo and the crude mixture was separated by column chromatography (petroleum ether/ethyl acetate 10:1) to give the product **5a** as a yellow solid (75 mg, 124 μmol, 11%). ¹H NMR (600.13 MHz, CDCl₃, 295 K): δ [ppm] = 8.74 (s, 4H). ¹³C NMR (150.90 MHz, CDCl₃, 295 K): δ [ppm] = 112.7, 125.3, 126.1, 130.7, 141.1, 153.8. Residual ¹³C signals of N-C-N- and CF₃-groups could not be detected due to coupling to fluorine groups and low solubility. ¹⁹F NMR (376.27 MHz, CDCl₃, 295 K): δ [ppm] = -69.0 (s, 6F). HRMS (MALDI⁻): calcd for C₂₄H₄³⁵Cl₃³⁷Cl₁F₆N₄ [M]⁻: 603.9065; found: 603.9059. Redox potentials measured against SCE in THF: E_{red1} = -0.18 V, E_{red2} = -0.49 V.

Preparation of compound 5b:

Triethylamine (414 μL , 2.97 mmol, 2.8 equiv.) and pentafluoropropionic anhydride (526 μL , 2.66 mmol, 2.5 equiv.) were added to a solution of DPDI-Cl (**4**) (476 mg, 1.06 mmol, 1 equiv.) in dioxane (10 mL) and the solution was refluxed for 72 h. After cooling to r.t., the solvent was removed in vacuo and the residue was washed thoroughly with water (200 mL). The crude compound was recrystallized in hot ethanol to afford **5b** as a yellow solid (170 mg, 241 μmol , 23%). $^1\text{H-NMR}$ (600.13 MHz, CDCl_3 , 295 K): δ [ppm] = 8.76 (s, 4H). $^{13}\text{C-NMR}$ (150.90 MHz, CDCl_3 , 295 K): δ [ppm] = 112.6, 125.3, 126.1, 130.8, 141.1, 153.8, 156.1. Residual ^{13}C -signals of the perfluorinated pentyl groups could not be detected due to coupling to fluorine groups. $^{19}\text{F-NMR}$ (376.27 MHz, CDCl_3 , 295 K): δ [ppm] = -81.4 (t, $^3J_{\text{F-F}} = 1.75$ Hz, 6F), -116.0 (bs, 4F). HRMS (MALDI $^-$): calcd for $\text{C}_{26}\text{H}_4^{35}\text{Cl}_3^{37}\text{Cl}_1\text{F}_{10}\text{N}_4$ [M] $^-$: 703.9001; found: 703.9006. Redox potentials measured against SCE in THF: $E_{\text{red1}} = -0.18$ V, $E_{\text{red2}} = -0.49$ V.

Preparation of compound 5c:

Triethylamine (217 μmol , 1.56 mmol, 2.8 equiv.) and perfluorobutryl chloride (207 μL , 1.39 mmol, 2.5 equiv.) were added to a solution of DPDI-Cl (**4**) (250 mg, 0.56 mmol, 1 equiv.) in THF (10 mL) and the solution was refluxed for 72 h. After cooling to r.t., the solvent was removed in vacuo and the residue was washed thoroughly with water (200 mL) and the crude product purified by column chromatography (petroleum ether/ethyl acetate 10:1) to give **5c** as a yellow solid (54 mg, 76 μmol , 14%). $^1\text{H-NMR}$ (600.13 MHz, CDCl_3 , 295 K): δ [ppm] = 8.77 (s, 4H). $^{13}\text{C-NMR}$ (150.90 MHz, CDCl_3 , 295 K): δ [ppm] = 112.5, 125.3, 126.1, 130.8, 141.1, 153.7. Residual ^{13}C -signals of the N-C-N- and perfluorinated propyl-groups could not be detected due to coupling to fluorine groups. $^{19}\text{F-NMR}$ (376.27 MHz, CDCl_3 , 295 K): δ [ppm] = -80.1 (t, $^3J_{\text{F-F}} = 9.03$ Hz, 6F), -114.0-114.1 (m, 4F), -125.4 (bs, 4F). HRMS (MALDI $^-$): calcd for $\text{C}_{28}\text{H}_4^{35}\text{Cl}_3^{37}\text{Cl}_1\text{F}_{14}\text{N}_4$ [M] $^-$: 803.8937; found: 803.8932. Redox potentials measured against SCE in THF: $E_{\text{red1}} = -0.19$ V, $E_{\text{red2}} = -0.49$ V.

Preparation of compound 5d:

DPDI-Cl (**4**) (100 mg, 0.223 mmol, 1 equiv.) was dissolved in 5 mL triethylorthoformate and 1 mL of formic acid was added. The solution was stirred for 3 d at 110 $^\circ\text{C}$. After cooling to r.t., the volatiles were removed in vacuo and residue was washed with water, MeOH and pentane. The pure compound **5d** was isolated as a yellow powder (25 mg, 0.053 mmol, 24%). $^1\text{H-NMR}$ (600.13 MHz, CDCl_3 , 295 K): δ [ppm] = 10.01 (s, 2H), 8.59 (s, 4H). $^{13}\text{C-NMR}$ could not be measured due to low solubility. HRMS (MALDI $^-$): calcd for $\text{C}_{22}\text{H}_6^{35}\text{Cl}_3^{37}\text{Cl}_1\text{N}_4$ [M] $^-$: 467.9317; found: 467.9315. Redox potentials measured against SCE in THF: $E_{\text{red1}} = -0.383$ V, $E_{\text{red2}} = -0.681$ V.

Theoretical methods

Frontier orbitals and electron affinities: The DFT calculations to obtain orbital energies and electron affinities were carried out using ORCA 4.0.1 program package.^[65] B3LYP was employed as functional,^[66,67] a def2-SVP basis set was used for all atoms during geometry optimizations.^[68,69] Every optimization was verified by frequency calculations. All other properties were calculated using a def2-QZVPP basis set.^[70]

Vertical transitions: Calculations of the vertical excitation energies (VEE) and vertical de-excitation energies (VDE), employing B3LYP together with the def2-TZVPP basis, have been carried out using the Turbomole program package V7.2^[71,72] using default conver-

gence criteria for both the response equations and the geometry convergence. Accurate geometries for the Franck-Condon simulations were obtained with tightened thresholds of 10^{-9} and employing D_2 symmetry.^[48] The calculations of the vibronic (Franck-Condon) spectra were conducted using the HOTFCHT program.^[73-75]

Interconversion energies: The geometries and their relative energies have been computed using the Turbomole program V7.2. PBE0 was employed as functional together with def2-TZVP basis and the RI approximation (RI-J). The stationary points were verified with analytical second derivatives.

Acknowledgements

This work has been supported by the Deutsche Forschungsgemeinschaft (DFG) within the collaborative research centre SFB1249 "N-Heteropolycycles as Functional Materials" (Projects A02, B07, and C01). Open access funding enabled and organized by ProjektDEAL.

Conflict of interest

The authors declare no conflict of interest.

Keywords: halogens • perylenes • radicals • synthetic methods • UV/Vis spectroscopy

- [1] W. Herbst, K. Hunger, *Industrial Organic Pigments*, Wiley-VCH Verlag, Weinheim, **2004**.
- [2] F. Würthner, *Chem. Commun.* **2004**, 0, 1564–1579.
- [3] F. Würthner, C. R. Saha-Möller, B. Fimmel, S. Ogi, P. Leowanawat, D. Schmidt, *Chem. Rev.* **2016**, *116*, 962–1052.
- [4] C. Huang, S. Barlow, S. R. Marder, *J. Org. Chem.* **2011**, *76*, 2386–2407.
- [5] X. Zhan, A. Facchetti, S. Barlow, T. J. Marks, M. A. Ratner, M. R. Wasielewski, S. R. Marder, *Adv. Mater.* **2011**, *23*, 268–284.
- [6] R. Jiang, Z. Xue, Y. Lee, Z. Qin, Y. Li, D. Zhu, *Eur. J. Org. Chem.* **2014**, *23*, 5004–5009.
- [7] C. Li, H. Wonneberger, *Adv. Mater.* **2012**, *24*, 613–636.
- [8] D.-J. Liaw, K.-L. Wang, Y.-C. Huang, K.-R. Lee, J.-Y. Lai, C.-S. Ha, *Prog. Polym. Sci.* **2012**, *37*, 907–974.
- [9] W. Jiang, Y. Li, Z. Wang, *Acc. Chem. Res.* **2014**, *47*, 3135–3147.
- [10] Y. Avlasevich, C. Li, K. Müllen, *J. Mater. Chem.* **2010**, *20*, 3814–3826.
- [11] L. Chen, C. Li, K. Müllen, *J. Mater. Chem. C* **2014**, *2*, 1938–1956.
- [12] N. Soh, T. Ueda, *Talanta* **2011**, *85*, 1233–1237.
- [13] A. Nowak-Król, F. Würthner, *Org. Chem. Front.* **2019**, *6*, 1272–1318.
- [14] M. Sun, K. Müllen, M. Yin, *Chem. Soc. Rev.* **2016**, *45*, 1513–1528.
- [15] G. Zhang, J. Zhao, P. C. Y. Chow, K. Jiang, J. Zhang, Z. Zhu, J. Zhang, F. Huang, H. Yan, *Chem. Rev.* **2018**, *118*, 3447–3507.
- [16] A. Nowak-Król, K. Shoyama, M. Stolte, F. Würthner, *Chem. Commun.* **2018**, *54*, 13763.
- [17] C. Yan, S. Barlow, Z. Wang, H. Yan, A. K.-Y. Jen, S. R. Marder, X. Zhan, *Nat. Rev. Mater.* **2018**, *3*, 18003.
- [18] F. Würthner, *Pure Appl. Chem.* **2006**, *78*, 2341–2349.
- [19] M. Queste, C. Cadiou, B. Pagoaga, L. Giraudet, N. Hoffmann, *New J. Chem.* **2010**, *34*, 2537.
- [20] F. Würthner, P. Osswald, R. Schmidt, T. E. Kaiser, H. Mansikkamaki, M. Könemann, *Org. Lett.* **2006**, *8*, 3765–3768.
- [21] R. Schmidt, J. H. Oh, Y.-S. Sun, M. Deppisch, A.-M. Krause, K. Radacki, H. Braunschweig, M. Könemann, P. Erk, Z. Bao, F. Würthner, *J. Am. Chem. Soc.* **2009**, *131*, 6215–6228.
- [22] P. Leowanawat, A. Nowak-Król, F. Würthner, *Org. Chem. Front.* **2016**, *3*, 537–544.
- [23] M. J. Lin, M. Schulze, K. Radacki, F. Würthner, *Chem. Commun.* **2013**, *49*, 9107–9109.

- [24] T. Teraoka, S. Hiroto, H. Shinokubo, *Org. Lett.* **2011**, *13*, 2532–2535.
- [25] X. Li, H. Wang, J. A. Schneider, Z. Wei, W.-Y. Lai, W. Huang, F. Wudl, Y. Zheng, *J. Mater. Chem. C* **2017**, *5*, 2781–2785.
- [26] W. Yue, W. Jiang, M. Böckmann, N. L. Doltsinis, Z. Wang, *Chem. Eur. J.* **2014**, *20*, 5209–5213.
- [27] S. Nakazono, S. Easwaramoorthi, D. Kim, H. Shinokubo, A. Osuka, *Org. Lett.* **2009**, *11*, 5426–5429.
- [28] G. Battagliarin, Y. Zhao, C. Li, K. Müllen, *Org. Lett.* **2011**, *13*, 3399–3401.
- [29] G. Battagliarin, C. Li, V. Enkelmann, *Org. Lett.* **2011**, *13*, 3012–3015.
- [30] J. Wu, D. He, L. Zhang, Y. Liu, X. Mo, J. Lin, H. J. Zhang, *Org. Lett.* **2017**, *19*, 5438–5441.
- [31] N. Zink-Lorrie, E. Font-Sanchis, Á. Sastre-Santos, F. Fernández-Lázaro, *Org. Chem. Front.* **2017**, *4*, 2016–2021.
- [32] S. Seifert, D. Schmidt, F. Würthner, *Chem. Sci.* **2015**, *6*, 1663–1667.
- [33] Y. Kumar, S. Kumar, S. Kumar Keshri, J. Shukla, S. S. Singh, T. S. Thakur, M. Denti, A. Facchetti, P. Mukhopadhyay, *Org. Lett.* **2016**, *18*, 472–475.
- [34] M. Sadrai, G. R. Bird, J. A. Potenza, H. J. Schugar, *Acta Crystallogr. Sect. C* **1990**, *46*, 637.
- [35] M. Gsänger, J. H. Oh, M. Könemann, H. W. Höffken, A. Krause, Z. Bao, F. Würthner, *Angew. Chem. Int. Ed.* **2010**, *49*, 740–743; *Angew. Chem.* **2010**, *122*, 752.
- [36] T. Riehm, G. De Paoli, A. E. Konradsson, L. De Cola, H. Wadepohl, L. H. Gade, *Chem. Eur. J.* **2007**, *13*, 7317–7329.
- [37] M. Matena, T. Riehm, M. Stöhr, T. A. Jung, L. H. Gade, *Angew. Chem. Int. Ed.* **2008**, *47*, 2414–2417; *Angew. Chem.* **2008**, *120*, 2448–2451.
- [38] S. Blankenburg, E. Rauls, W. G. Schmidt, *J. Phys. Chem. Lett.* **2010**, *1*, 3266–3270.
- [39] M. Matena, M. Stöhr, T. Riehm, J. Björk, S. Martens, M. S. Dyer, M. Persson, J. Lobo-Checa, K. Müller, M. Enache, et al., *Chem. A Eur. J.* **2010**, *16*, 2079–2091.
- [40] J. Björk, M. Matena, M. S. Dyer, M. Enache, J. Lobo-Checa, L. H. Gade, T. A. Jung, M. Stöhr, M. Persson, *Phys. Chem. Chem. Phys.* **2010**, *12*, 8815–8821.
- [41] S. C. Martens, T. Riehm, S. Geib, H. Wadepohl, L. H. Gade, *J. Org. Chem.* **2011**, *76*, 609–617.
- [42] S. C. Martens, U. Zschieschang, H. Wadepohl, H. Klauk, L. H. Gade, *Chem. Eur. J.* **2012**, *18*, 3498–3509.
- [43] S. Geib, S. C. Martens, M. Märken, A. Rybina, H. Wadepohl, L. H. Gade, *Chem. Eur. J.* **2013**, *19*, 13811–13822.
- [44] S. Geib, U. Zschieschang, M. Gsänger, M. Stolte, F. Würthner, H. Wadepohl, H. Klauk, L. H. Gade, *Adv. Funct. Mater.* **2013**, *23*, 3866–3874.
- [45] L. Hahn, S. Öz, H. Wadepohl, L. H. Gade, *Chem. Commun.* **2014**, *50*, 4941–4943.
- [46] Y. Shi, H. Wei, Y. Liu, *J. Mol. Struct.* **2015**, *1083*, 65–71.
- [47] L. Hahn, A. Hermannsdorfer, B. Günther, T. Wesp, B. Bühler, U. Zschieschang, H. Wadepohl, H. Klauk, L. H. Gade, *J. Org. Chem.* **2017**, *82*, 12492–12502.
- [48] S. Höfener, B. Günther, M. E. Harding, L. H. Gade, *J. Phys. Chem. A* **2019**, *123*, 3160–3169.
- [49] Y. Zagranyski, L. Chen, D. Jänsch, T. Gessner, C. Li, K. Müllen, *Org. Lett.* **2014**, *16*, 2814–2817.
- [50] A. Insuasty, S. Maniam, S. J. Langford, *Chem. Eur. J.* **2019**, *25*, 7058–7073.
- [51] Z. Xie, F. Würthner, *Org. Lett.* **2010**, *12*, 3204–3207.
- [52] P. Osswald, D. Leusser, D. Stalke, F. Würthner, *Angew. Chem. Int. Ed.* **2005**, *44*, 250–253; *Angew. Chem.* **2005**, *117*, 254–257.
- [53] M. M. Safont-Sempere, P. Osswald, M. Stolte, M. Grüne, M. Renz, M. Kaupp, K. Radacki, H. Braunschweig, F. Würthner, *J. Am. Chem. Soc.* **2011**, *133*, 9580–9591.
- [54] A. Nowak-Król, M. I. S. Röhr, D. Schmidt, F. Würthner, *Angew. Chem. Int. Ed.* **2017**, *56*, 11774–11778; *Angew. Chem.* **2017**, *129*, 11936–11940.
- [55] M. M. Safont-Sempere, P. Osswald, K. Radacki, F. Würthner, *Chem. Eur. J.* **2010**, *16*, 7380–7384.
- [56] M. M. Safont-Sempere, V. Stepanenko, M. Lehmann, F. Würthner, *J. Mater. Chem.* **2011**, *21*, 7201–7209.
- [57] Z. Xie, V. Stepanenko, K. Radacki, F. Würthner, *Chem. Eur. J.* **2012**, *18*, 7060–7070.
- [58] E. Fron, G. Schweitzer, P. Osswald, F. Würthner, P. Marsal, D. Beljonne, K. Müllen, F. C. De Schryver, M. Van der Auweraer, *Photochem. Photobiol. Sci.* **2008**, *7*, 1509–1521.
- [59] P. Osswald, F. Würthner, *J. Am. Chem. Soc.* **2007**, *129*, 14319–14326.
- [60] I. Seguy, P. Jolinat, P. Destruel, R. Mamy, H. Allouchi, C. Courseille, M. Co-trait, H. Bock, *ChemPhysChem* **2001**, *2*, 448–452.
- [61] M. J. van Setten, F. Weigend, F. Evers, *J. Chem. Theory Comput.* **2013**, *9*, 232–246.
- [62] B. C. Lin, C. P. Cheng, Z. P. M. Lao, *J. Phys. Chem. A* **2003**, *107*, 5241–5251.
- [63] L. Hahn, F. Maaß, T. Bleith, U. Zschieschang, H. Wadepohl, H. Klauk, P. Tegeder, L. H. Gade, *Chem. Eur. J.* **2015**, *21*, 17691–17700.
- [64] G. R. Fulmer, A. J. M. Miller, N. H. Sherden, H. E. Gottlieb, A. Nudelman, B. M. Stoltz, J. E. Bercaw, K. I. Goldberg, *Organometallics* **2010**, *29*, 2176–2179.
- [65] F. Neese, *Wiley Interdiscip. Rev.: Comput. Mol. Sci.* **2012**, *2*, 73–78.
- [66] A. D. Becke, *J. Chem. Phys.* **1993**, *98*, 5648–5652.
- [67] A. D. Becke, *J. Chem. Phys.* **1993**, *98*, 1372–1377.
- [68] C. Lee, W. Yang, R. G. Parr, *Phys. Rev. B* **1988**, *37*, 785–789.
- [69] F. Weigend, M. Häser, H. Patzelt, R. Ahlrichs, *Chem. Phys. Lett.* **1998**, *294*, 143–152.
- [70] F. Weigend, R. Ahlrichs, *Phys. Chem. Chem. Phys.* **2005**, *7*, 3297.
- [71] TURBOMOLE V7.2 2017, A Development Of University Of Karlsruhe And Forschungszentrum Karlsruhe GmbH.
- [72] R. Ahlrichs, M. Bär, M. Häser, H. Horn, C. Kölmel, *Chem. Phys. Lett.* **1989**, *162*, 165–169.
- [73] R. Berger, C. Fischer, M. Klessinger, *J. Phys. Chem. A* **1998**, *102*, 7157–7167.
- [74] R. Berger, M. Klessinger, *J. Comput. Chem.* **1997**, *18*, 1312–1319.
- [75] H.-C. Jankowiak, J. L. Stuber, R. Berger, *J. Chem. Phys.* **2007**, *127*, 234101.

Manuscript received: July 26, 2019

Revised manuscript received: August 30, 2019

Accepted manuscript online: September 17, 2019

Version of record online: October 22, 2019